Geochemistry Geophysics Geosystems G3

Article
Volume 13, Number 12
6 December 2012
Q12001, doi:10.1029/2012GC004369
ISSN: 1525-2027

Published by AGU and the Geochemical Society

Waveform modeling of shear wave splitting from anisotropic models in Iceland

Yuanyuan V. Fu
Department of Earth and Atmospheric Sciences, University of Houston, Houston, Texas 77204, USA

Now at Institute of Earthquake Science, China Earthquake Administration, Beijing 100036, China (fuyuanies@163.com)

Aibing Li
Department of Earth and Atmospheric Sciences, University of Houston, Houston, Texas 77204, USA

Garrett Ito
Department of Geology and Geophysics, School of Ocean and Earth Science and Technology, University of Hawai'i at Mānoa, Honolulu, Hawai'i 96822, USA

Shu-Huei Hung
Department of Geosciences, National Taiwan University, Taipei 10617, Taiwan

[1] No quantitative model of seismic anisotropy beneath Iceland has yet explained the observed shear wave splitting results in Iceland. In this study we explore the structure of mantle seismic anisotropy associated with plume ridge interaction beneath Iceland by modeling synthetic waveforms using a pseudo-spectral method. First, predicted SKS waveforms are shown to produce shear wave splitting results for two anisotropic layers that are in generally agreement with analytic solutions. Next, simple models in which anisotropy are imposed at different depths and geographic regions around Iceland are used to examine different hypothesized effects of plume-ridge interaction. The model that is designed to represent crystallographic fabric due to mantle deformation associated with lithosphere spreading in western Iceland and along-axis, channeled asthenospheric flow in eastern Iceland can predict the distinct shear wave splitting observations on the east and west sides of the island. Last, we analyze geodynamic models that simulate 3-D mantle flow and evolution of mineral fabric. The predicted fast directions of shear wave splitting from the models with realistic spreading rate (10 km/Myr) and broad range of plume viscosities are consistent with the observations in central and eastern Iceland. However, because these models are symmetric about the ridge, none of them can predict the observed shear wave splitting results in western Iceland.

Components: 8600 words, 11 figures, 2 tables.

Keywords: Iceland; seismic anisotropy; shear wave splitting.

Index Terms: 7245 Seismology: Mid-ocean ridges; 8120 Tectonophysics: Dynamics of lithosphere and mantle: general (1213).

Received 2 August 2012; **Revised** 19 October 2012; **Accepted** 26 October 2012; **Published** 6 December 2012.

Fu, Y. V., A. Li, G. Ito, and S.-H. Hung (2012), Waveform modeling of shear wave splitting from anisotropic models in Iceland, *Geochem. Geophys. Geosyst.*, *13*, Q12001, doi:10.1029/2012GC004369.

1. Introduction

[2] Seismic anisotropy originating from lattice preferred orientation (LPO) of mantle minerals provides information on mantle flow and tectonic deformation in the Earth's interior [*Silver*, 1996]. In the ideal situation of simple shear, the α-axis of dry olivine tends to align parallel to the flow direction for large strains (shear strain >2), or parallel to the maximum principal, finite strain direction for small strains (shear strain <0.5) [e.g., *N. I. Christensen*, 1984; *Mainprice and Silver*, 1993; *Zhang and Karato*, 1995]. Shear wave splitting (SWS) is a method for detecting seismic anisotropy in the upper mantle and involves measuring the delay time between arrivals of the two quasi-shear waves and the direction of polarization of the fast shear wave. Due to its simplicity and high lateral resolution, SWS has been widely used to assess the orientation and magnitude of mantle deformation [e.g., *Kind et al.*, 1985; *Silver and Chan*, 1988; *Vinnik et al.*, 1989, 1992; *Fouch et al.*, 2004; *Fu et al.*, 2008].

[3] Iceland, located on the mid-Atlantic ridge, is an ideal place to study the plume-ridge interaction (Figure 1). Seismic anisotropy in Iceland has been well studied from shear wave splitting and surface wave tomography [*Bjarnason et al.*, 1996, 2002; *Li and Detrick*, 2003; *Xue and Allen*, 2005]. Studies of shear wave splitting usually adopt the method of *Wolfe and Silver* [1998] to calculate the station-average splitting parameters and generally found N-S oriented fast directions in western Iceland and NNW-SSE oriented fast splitting directions in eastern and central Iceland [*Bjarnason et al.*, 1996, 2002; *Li and Detrick*, 2003; *Xue and Allen*, 2005] (Figure 1). Although most of splitting observations from each study are consistent with each other, there are still exceptions at some stations. For example, at a station in central Iceland, the splitting direction from *Xue and Allen* [2005] is NW-SE, which is almost perpendicular to NE-SW observed by *Li and Detrick* [2003] and NNE-SSW observed at nearby station by *Bjarnason et al.* [2002]. The origin of the different observations of seismic anisotropy is still not well known and several scenarios have been proposed to interpret the splitting observations. *Bjarnason et al.* [2002] explain their splitting results by the shear between the North American or Eurasian plate and background mantle flow. *Li and Detrick* [2003] attribute the teleseismic splitting to the background mantle flow deeper than 100 km to reconcile the difference of results between the shear wave splitting and surface wave. *Xue and Allen* [2005] interpret their splitting results as the ridge-channeled flow. Such discrepancy in the interpretation of shear wave splitting observations indicates that seismic anisotropy is complicated beneath Iceland.

[4] Plume-ridge interaction involves mantle deformation and hence anisotropy that is spatially heterogeneous. Different mechanisms that may contribute to the seismic anisotropy include plate spreading [*Francis*, 1969; *Blackman et al.*, 1996], channeled flow of the plume along the mid-Atlantic ridge [*Vogt*, 1976; *Yale and Morgan*, 1998; *Albers and Christensen*, 2001], radial flow away from the plume center [*White and Lovell*, 1997; *Ito*, 2001], and mantle flow associated with the absolute plate movement [*Vinnik et al.*, 1989]. The shear wave splitting measurements on Iceland [*Bjarnason et al.*, 1996, 2002; *Li and Detrick*, 2003; *Xue and Allen*, 2005] might be generated from multiple different mechanisms. Moreover, recent of studies of plastic deformation and recrystallization in olivine polycrystals show that LPO aligns with the flow direction (for large strains) only if the finite strain axis after infinite strain is aligned with the flow direction, and if the LPO is able to rotate as quickly as the "infinite strain axis" in a situation of variable flow [*Kaminski and Ribe*, 2002]. Such circumstances are not always met in strongly heterogeneous flows such as that anticipated to be present beneath Iceland. Considering this effect makes inferences about the nature of mantle flow beneath Iceland from seismic observations even less straightforward.

[5] In this study we explore the form and causes of mantle anisotropy beneath Iceland by examining different models of mantle anisotropy, generating synthetic waveforms using the multidomain, pseudo-spectral method [*Hung and Forsyth*, 1998], and comparing synthetic and observed SWS results. The pseudo-spectral method has been shown to be accurate in simulating the propagation of finite-frequency, seismic waves through a heterogeneous mantle [e.g., *Hung and Forsyth*, 1999; *Hung et al.*, 2000; *Fischer et al.*, 2005]. We first employ this method to a two-layer, anisotropic model to validate the results against analytical solutions of SWS [*Silver and Savage*, 1994]. We then examine simple models in which anisotropy is imposed to simulate different mechanisms of plume ridge interaction. Finally we examine more realistic, three-dimensional (3-D) geodynamic models of mantle flow due to plume-ridge interaction as well as the formation of LPO

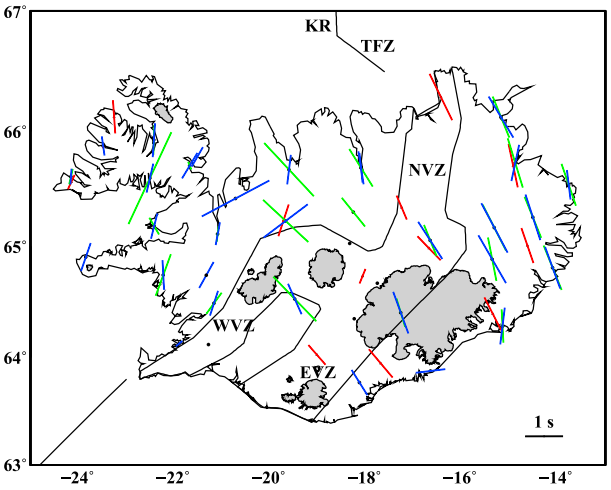

Figure 1. Tectonic map of Iceland. Thick black lines outline the volcanic zones in Iceland and ridge segments in the Atlantic. Shaded areas mark the locations of major icecaps. The Iceland hot spot is currently centered beneath the largest icecap in southeast. Splitting parameters are shown as blue bars at the ICEMELT stations from *Bjarnason et al.* [2002], red bars at the HOT SPOT stations from *Li and Detrick* [2003], and green bars at the HOT SPOT and SIL stations from *Xue and Allen* [2005]. WVZ, Western Volcanic Zone; EVZ, Eastern Volcanic Zone; NVZ, Northern Volcanic Zone; RR, Reykjanes Ridge; KR, Kolbeinsey Ridge; TFZ, Tjornes Fracture Zone.

in an olivine-enstatite aggregate and the resulting seismic anisotropy. Shear wave splitting parameters are obtained by analyzing the generated synthetic waveforms and are compared with the observed ones to identify the best model for Iceland.

2. Method

[6] We adopt the multidomain pseudo-spectral method developed by *Hung and Forsyth* [1998] in generating synthetic shear wave waveforms. This method can simulates seismic wave propagation in 3-D anisotropic media and has been used by *Fischer et al.* [2005] in evaluating laterally varied anisotropic models. This method has an advantage over other ray-tracing methods [e.g., *Booth and Crampin*, 1983; *Kendall and Thomson*, 1993; *Rümpker and Silver*, 1998; *Abt and Fischer*, 2008] because it can fully account for the frequency-dependent interaction of seismic wavefields with three-dimensional anisotropic structure. The wavefield variables are approximated with Fourier series in the horizontal directions and Chebyshev polynomials in the vertical direction and updated in time domain by a fourth-order Runge Kutta method. The computer program for this method is run on parallel processors and is numerically efficient.

[7] After synthetic waveforms are calculated, we apply the method of *Silver and Chan* [1991] to estimate the shear wave splitting parameters, fast polarization direction and delay time. First, the horizontal components of seismograms are rotated to the radial and transverse components. The method then searches over fast polarization directions from −90° to 90° (positive clockwise from north) and delay times in a range of 0–8 s to find the pair that results in the most singular covariance matrix by minimizing the lesser of the two eigenvalues. The particle motion of each phase is initially elliptical, which is indicative of SWS, and then becomes roughly linear after the effects of SWS are removed using the best splitting parameters.

3. Shear Wave Splitting From a Two-Layer Anisotropic Model

[8] Before examining anisotropy from models of Iceland, we feel it is necessary to evaluate whether the adopted waveform method can accurately and effectively predict synthetic SWS results. We therefore compare SWS results for a two-layer anisotropic model from the synthetic waveform method with analytical solutions of layered anisotropy. Each layer of the model is characterized by hexagonal anisotropy of 4% with a horizontal symmetry axis oriented in the azimuth of high velocity direction, which makes a total splitting time of 1 s. The fast-axes for the top and bottom layers are N20°W and N70°W, respectively. The total model space spans 511 km × 511 km horizontally and 252 km vertically with the bottom 32 km being isotropic and the model is discretized into 512 × 512 × 64 mesh elements (Figure 2). We use a P wave velocity of 8 km/s, an S wave velocity of 4.5 km/s, a density of 3300 kg/m^3, and assume a plane SV wave as the incident wave at a depth of 220 km. Absorbing boundary conditions are applied on all sides of the box to minimize unwanted reflections from boundaries [*Cerjan et al.*, 1985; *Hung and Forsyth*, 1998].

[9] We show an example of synthetic waveforms with a dominant period of 4 s recorded at the surface, as well as the corresponding shear wave splitting measurement in Figure 3. A vertically incident plane wave is imposed at zero time with a particle motion polarized at an azimuth of 90° (clockwise from *Y* axis). The splitting parameters are well constrained. The obtained apparent fast direction is N43°W,

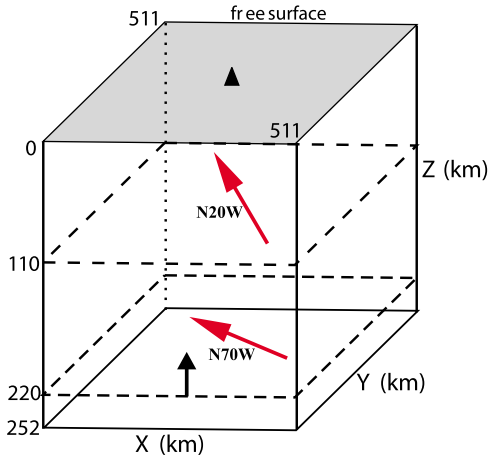

Figure 2. The geometry of the model space for the two-layer anisotropic models (bases outlined by dashed lines). Solid triangles indicate the receiver located at the free surface. The black arrow indicates the incident wave at 220 km. The red arrows show the fast directions in the top and bottom layer, respectively.

an angle that is intermediate between the fast directions in the top (N20°W) and bottom (N70°W) layer; the apparent delay time is less than the sum of the delay times of the two layers.

[10] This method of waveform modeling allows us to investigate the evolution of the wavefield and the changes in splitting parameters with depth (Figure 4). A shear wave splits into a fast and slow wave when it encounters an anisotropic boundary. Theoretically, as the wavefield enters the top anisotropic layer, the fast and slow waves should split again and form four phases [*Yardley and Crampin*, 1991]. To better view the interference of fast and slow waves generated at each anisotropic boundary, we produce synthetic waveforms for a wave with an initial polarization of N10°E and an artificially short period of 1 s. Figure 4 clearly reveal that waveform changes with depth. The wave on the transverse component has small amplitude and a simple pulse in the second layer beneath 110 km and evolves to have one peak and one trough at 55 km to surface. On the radial component, a single pulse wave at depth evolves to two separated waves at the surface. The fast direction beneath 110 km is very close to the imposed fast axis in the second layer and it becomes progressively closer to the fast axis of the top layer as the wavefield propagates upward through the layer. It is interesting to notice that the apparent delay time decreases near the base of the top layer and then increases toward the surface (Figure 4).

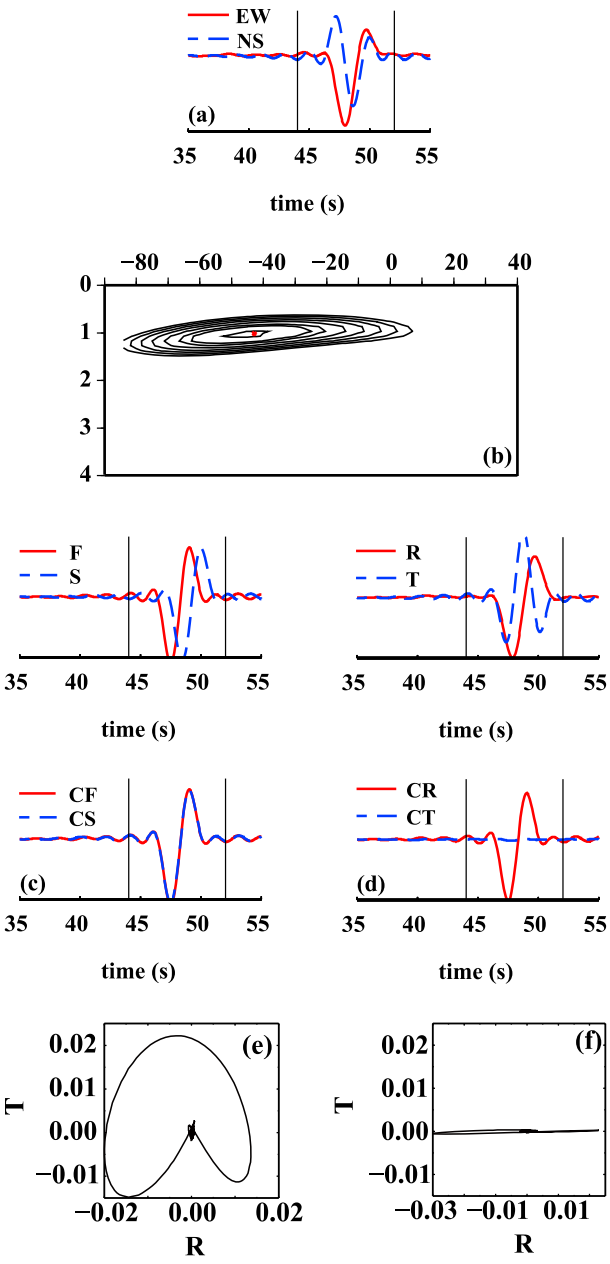

Figure 3. Splitting analysis of synthetic waveforms with a dominant period of 4 s and initial polarization of E-W from the two-layer anisotropic model shown in Figure 2. (a) Original waveforms of N-S and E-W components. (b) Contours of residual tangential energy are used to identify the optimum splitting parameters (red dot) in the fast direction and delay time space. The smallest contour indicates the 95% confidence level. (c) (top) Original and (bottom) corrected fast and slow components of motion. (d) (top) Original and (bottom) corrected radial and transverse components. (e) Original horizontal particle motion. (f) Corrected horizontal particle motion.

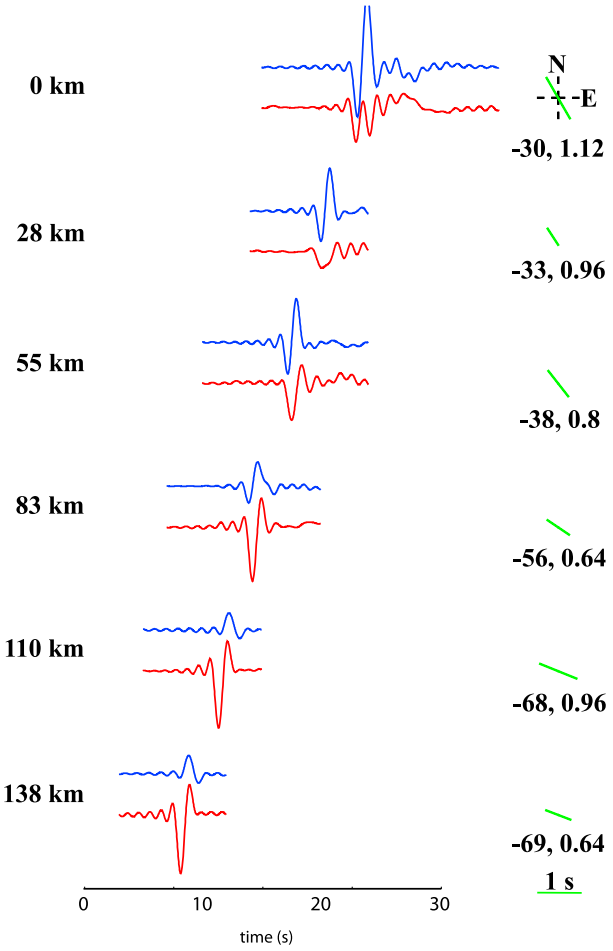

Figure 4. Synthetic waveforms on radial (red) and transverse (blue) components at a variety of depths and correspondent shear wave splitting results (green bars) from the two-layer anisotropic model. Fast direction is the first number on right in degrees and delay time is the second number in s. The orientation and length of the green bar indicate the fast direction and delay time, respectively.

[11] The apparent splitting parameters for the two-layer anisotropic model generally exhibit a $\pi/2$ dependence on the polarization of the incoming shear wave that varies between 0° and 180°. For comparison we use the formulas of *Silver and Savage* [1994] to calculate the apparent splitting parameters for the two-layer model. The predicted splitting parameters from the numerical method (with a wave period of 4 s) and the analytic method agree with each other in terms of general variation and $\pi/2$ periodicity as a function of initial shear wave polarization (Figure 5). The slightly smaller range of splitting parameters from the synthetic waveforms is probably due to finite-frequency wavefields used in the numerical simulation. The consistence in SWS predictions from the two methods confirms that the pseudo-spectral method is able to fully account for the propagation and development of wavefields in variable anisotropic structure.

4. Shear Wave Slitting From Simple Models

[12] Seismic anisotropy in Iceland could have contributions from plate spreading, ridge-parallel plume flow, shear between the plates and large-scale mantle flow, and mantle flows related to plume-ridge interaction. In this section we use simple models in which anisotropy is imposed to simulate the effects of these different contributions in order to identify what possible combinations could explain the observed

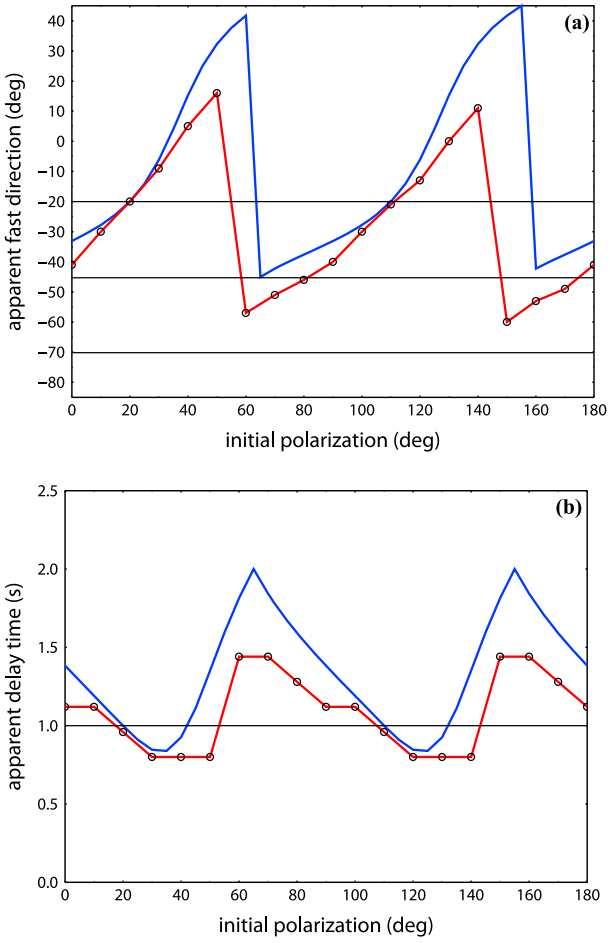

Figure 5. Predicted apparent (a) fast direction and (b) delay time as a function of incoming polarization direction. Black lines are the fast directions of the top (−20°) and bottom (−70°) layer and the delay time for each layer (both 1 s). Red lines are the splitting parameters from the full waveform method; blue lines are from the analytic solution.

shear wave splitting in Iceland. These models simulate various forms of anisotropy within the zone of a spreading center (oriented N20°E and of width 70 km), a plume in southeast just outside the ridge, a lithospheric layer of the North American and Eurasian plates, and the asthenospheric mantle beneath the plates (Figures 6a, 6c, 6e, 7a, and 7c). Each model has a horizontal dimension of 1024 km by 1024 km. The lithosphere thickness is set as 60 km according to the surface wave study of *Li and Detrick* [2006]. Synthetic waveforms are calculated at stations on the surface with a plane shear wave incident from the depth of 220 km in the model. The input shear wave has a period of 12 s and initial polarization of N30°E, which are consistent with the most representative waves in the observations [*Bjarnason et al.*, 2002; *Li and Detrick*, 2003; *Xue and Allen*, 2005]. The elastic constants are calculated for aggregates that are composed of 70% olivine and 30% orthopyroxene with a net anisotropy of 2% (unless otherwise noted). The parameters for each model are shown in Table 1.

[13] In the first model (SM1, Figure 6a), the fast direction in the lithosphere of eastern Iceland is assumed to align with the spreading direction, which is N70°W (N110°E), and perpendicular to the ridge axis. In the lithosphere of the ridge zone, anisotropy is assumed to be dominated by ridge-parallel cracks or melt pockets as suggested by surface wave tomography [*Li and Detrick*, 2003]. We therefore set the fast direction at the ridge as N20°E (also 2% anisotropy) to 60 km depth. In the lithosphere of western Iceland, the fast axis is also set as ridge parallel rather than perpendicular to the ridge. The reason for this choice is that the ridge was formerly located in western Iceland and has migrated eastward toward the current location in the past ~16 Myr [*Sæmundsson*, 1974; *Hardarson et al.*, 1997]. The ridge-parallel features can be a frozen fabric associated with the abandoned ridge segments in western Iceland. The asthenosphere is assumed to be isotropic except along the ridge axis and within the plume, where olivine α-axis is set as vertical.

[14] The fast directions of shear wave splitting calculated from model SM1 (Figure 6b) are N19°E in western Iceland and in the ridge axis zone, and N71°W in eastern Iceland. There is a transition across the western edge of the east Iceland, which is characterized by a relatively smooth westward change in the fast direction from N19°E to N53°W and delay time from 0.32 to 0.16 s. This transition is probably the effect of the Fresnel zone of the wave, which samples two different anisotropic regions. In western Iceland, the predicted N19°E fast direction is close to the observed average of N21°E [*Xue and Allen*, 2005] and largely parallel to the current and abandoned ridges. However, in eastern Iceland, the difference between the predicted fast direction (N71°W) and the observed average (N17°W) [*Xue and Allen*, 2005] is significant, indicating that the fabric associated with the plate spreading, as assumed in the model, cannot be a dominate mechanism for anisotropy in eastern Iceland.

[15] The second model (SM2, Figure 6c) has the same anisotropy structure as model SM1 except the asthenospheric layer in eastern Iceland is now anisotropic and has a fast orientation of N20°W. This anisotropy could be caused by olivine α-axes that are aligned parallel to flow from the plume center toward and along the ridge beneath eastern Iceland as suggested by *Vogt* [1976] and numerically simulated by *Albers and Christensen* [2001]. Shear wave splitting results from the synthetic waveforms calculated through this model (Figure 6d) reveal that the average fast direction changes from N19°E in western Iceland and the ridge zone to N40°W in eastern Iceland. The predicted fast direction in eastern Iceland is close to the observed shear wave splitting directions of N11°W to N30°W [*Li and Detrick*, 2003; *Xue and Allen*, 2005]. We also tested a very similar model but without the spreading-perpendicular fabric in the lithosphere of eastern Iceland, the results show that the fabric representing plume flow toward and along the ridge in the asthenosphere alone can predict shear wave splitting observations in eastern Iceland.

[16] The third model (SM3, Figure 6e) is much like model SM1 but anisotropy is present in the asthenosphere that is parallel to the absolute plate motions (APM) of the North American and the Eurasian plates [*Silver*, 1996]. The APM is N74°W for the North American plate beneath western Iceland and S51°W for the Eurasian plate beneath eastern Iceland [*Gripp and Gordon*, 1990]. For the Eurasian plate, the direction is poorly constrained because the plate velocity is not significantly different from zero. Since the velocity of the Eurasian plate is about one fourth of that of the North American plate [*Bjarnason et al.*, 2002], we set the strength of anisotropy in the bottom layer to be 0.5% beneath eastern Iceland and as 2% beneath western Iceland. The predicted fast directions from shear wave splitting are N79°W in western Iceland, N26°E in the ridge zone and N82°W in eastern Iceland (Figure 6f). Across the edges of the ridge, the fast directions and delay times both vary smoothly. These predicted fast directions

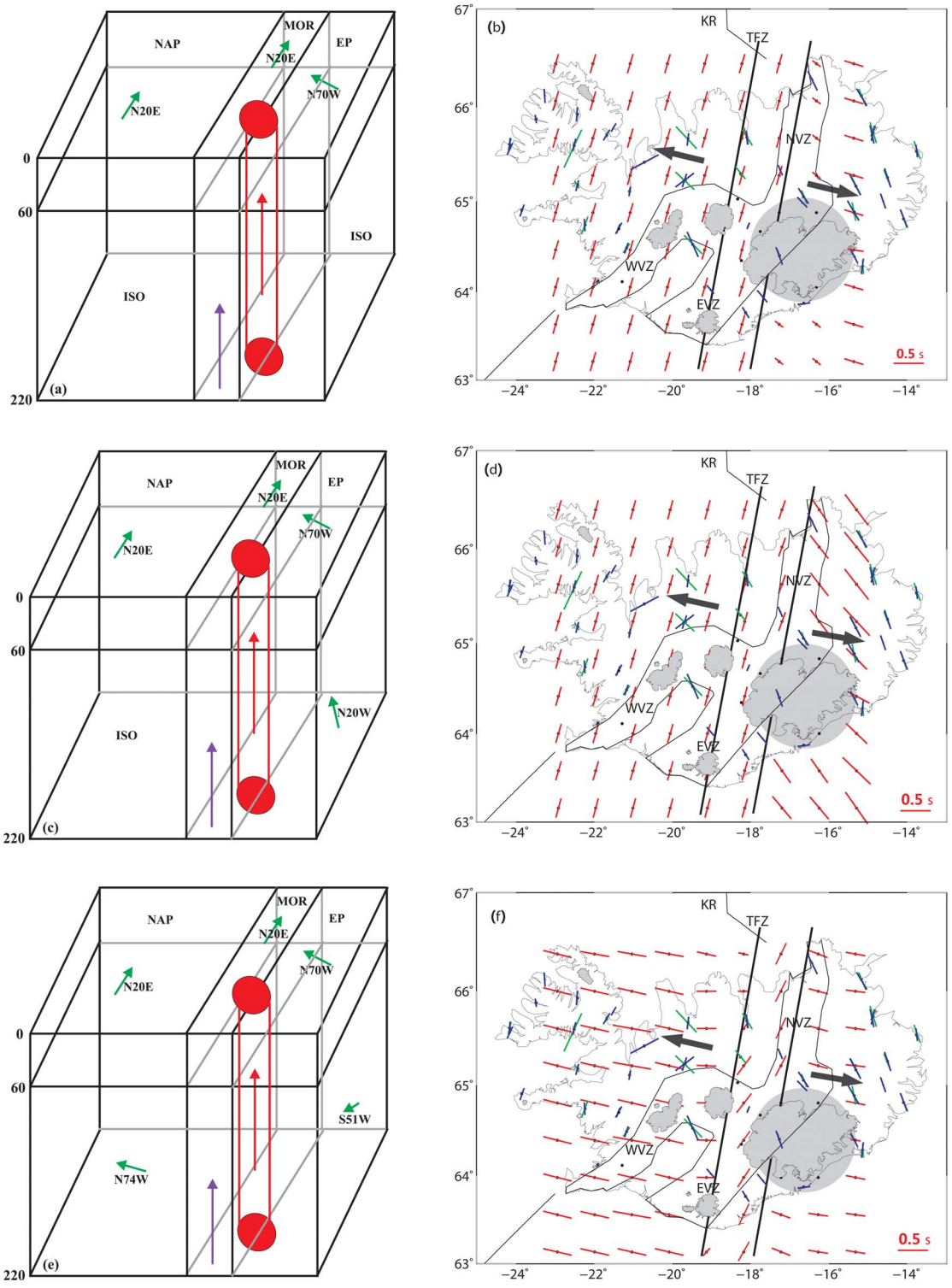

Figure 6. (a, c, and e) 3-D view of simple two-layer models (SM1, SM2 and SM3) which consider two or more basic anisotropic components and (b, d, and f) comparison of shear wave splitting results between predicted splitting parameters from the models (red bars oriented with fast direction and having length proportional to split time) and the real observations from *Bjarnason et al.* [2002] and *Li and Detrick* [2003] (blue bars) and *Xue and Allen* [2005] (green bars). The red cylinder represents the plume. The arrows show the assumed fast directions. The black arrows in Figures 6b, 6d, and 6f indicate the plate spreading direction. NAP, North American plate; MOR, Middle Ocean ridge; EP, Eurasian plate; ISO, isotropic.

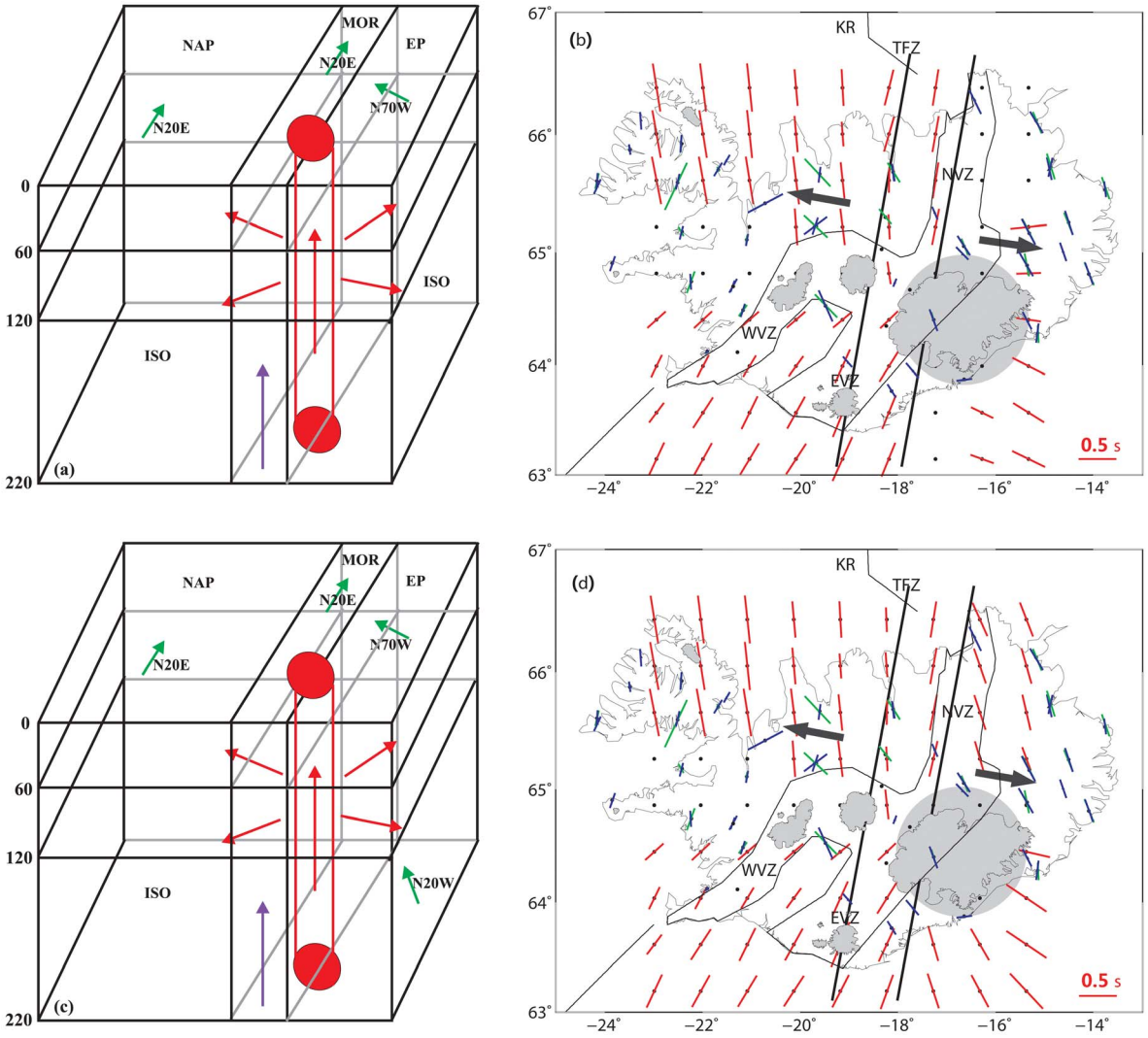

Figure 7. Same as Figure 6 but for two 3-layer models (SM4 and SM5) including a layer with radially oriented fast axes to simulate radial flow away from the plume center.

are almost perpendicular to the observed ones in both western and eastern Iceland.

[17] Another end-member type of asthenospheric flow is radial flow away from the plume center. This type of flow is similar to that simulated in geodynamic models that successfully predicted gravity anomalies along the Reykjanes Ridge [*Ribe et al.*, 1995; *Ito et al.*, 1996; *Ito*, 2001]. In the two models (SM4 and SM5) in Figure 7, we again

Table 1. Summary of Simple Model Parameters[a]

		Eastern Iceland (FD, AS)		Western Iceland (FD, AS)	
Model Name	Layers	Lithosphere	Asthenosphere	Lithosphere	Asthenosphere
SM1	2	N70°W, 2%	isotropic	N20°E, 2%	isotropic
SM2	2	N70°W, 2%	N20°W, 2%	N20°E, 2%	isotropic
SM3	2	N70°W, 2%	S51°W, 0.5%	N20°E, 2%	N74°W, 2%
SM4	3	N70°W, 2%	radial, 2% isotropic	N20°E, 2%	radial, 2% isotropic
SM5	3	N70°W, 2%	radial, 2% N20°W, 2%	N20°E, 2%	radial, 2% isotropic

[a]FD, fast direction; AS, anisotropy strength.

Table 2. Summary of Geodynamic Model Parameters

Model Name	Rayleigh Number	Half Spreading Rate (km/Myr)	Plume Radius (km)	Peak Plume Temperature (°C)
Radial				
GM1	**Error! Objects cannot be created from editing field codes.**	0	100	200
GM2	**Error! Objects cannot be created from editing field codes.**	10	100	200
Channel				
GM3	**Error! Objects cannot be created from editing field codes.**	1	58	300
GM4	**Error! Objects cannot be created from editing field codes.**	10	50	250

assume the olivine α-axes parallel mantle flow and both radiate away from the plume stem in the asthenosphere. Model SM4 and SM5 (Figures 7a and 7c) contain three layers, a top lithospheric layer having the same anisotropy of model SM1 (Figure 6a), a middle layer (60 km in thickness) having anisotropy directed radially from the plume and vertically within the plume, and a bottom layer in which the anisotropy differs between the two models. In model SM4 (Figure 7a), the bottom layer is isotropic except the vertical anisotropy in the plume and beneath the ridge. The bottom layer of model SM5 is the almost same as that of model SM4 except beneath eastern Iceland, where anisotropy is assumed with an orientation of N20°W to simulate the effects of flow from the plume toward and along the ridge axis.

[18] In model SM4, synthetic shear wave splitting results (Figure 7b) show a much more complicated pattern compared with the previous models. Little or no shear wave splitting is observed in northeastern Iceland and the middle part of western Iceland. A roughly radial pattern is found elsewhere, reflecting the input radial flow model. However, the radial pattern of anisotropy is not observed from shear wave splitting of real seismic data.

[19] In model SM5, the predicted fast SWS directions (Figure 7d) are similar to that of model SM4 (Figure 7b) except in northeastern Iceland, where the fast direction is N18°W. The anisotropy in northwestern and northeastern Iceland is now consistent with the observation. However, the radial pattern of the fast splitting directions in central and southern Iceland is not observed.

[20] These simple models were designed to test how SWS responds to different idealized structures of anisotropy due to different hypothesized effects of plume-ridge interaction. The findings reveal some insights as to the directions of anisotropy that are least and more likely to be present beneath Iceland; however, the shortcoming of the above exercise is that connection between the anisotropy and the mantle flow is assumed and not necessarily consistent with continuum mechanical theory. To overcome these limitations, we have developed geodynamic models and simulated wave propagation through them to obtain synthetic waveform and anisotropy.

5. Geodynamic Models

[21] The geodynamic models simulate the 3-D mantle flow and crystallographic evolution due to plume-ridge interaction. Mantle flow is computed by numerically solving the equations governing conservation of mass, momentum, and energy of a viscous fluid with zero Reynolds number and infinite Prandtl number using the mantle convection code, Citcom [*Moresi and Gurnis*, 1996; *Zhong et al.*, 2000]. Each model is contained in a 3-D Cartesian volume with depth of 400 km and horizontal dimensions of 1024 km by 1024 km. Mantle viscosity is an Arrhenius function of temperature- and pressure [e.g., *Ballmer et al.*, 2009] with reduced values of activation energy (150 $kJmol^{-1}$) and activation volume (volume of 5×10^{-6} m^3mol^{-1}) compared to laboratory estimates for dislocation creep [*Hirth and Kohlstaedt*, 2003] to simulate a power law rheology in steady state flows [*U. Christensen*, 1984]. A plume is imposed with a circular patch of a specified excess temperature on the bottom boundary directly beneath the ridge axis at $X = Y = 0$. Plate spreading (when present) is simulating by moving the top boundary in the X direction. The ridge is located at $X = 0$ and extends along the Y axis. The vertical sides of the box at $X = Y = 0$ are symmetry planes so only one quadrant of a full ridge-centered plume system is numerically modeled. The other vertical sides are free of deviatoric stress and open to flow. The parameters for each flow model are shown in Table 2.

[22] The LPO of olivine-enstate aggregates that develop along mantle flow paths is computed using

DRex [*Kaminski et al.*, 2004]. Just as in the public version of DRex, we evaluate LPO at a given location in the model by using a fourth order Runge-Kutta scheme to track the material backward along its 3-D flow path. Time along the flow path is discretized and the interpolated flow field at each point of the path is used to compute the LPO as it evolves to the final end point. We use the reference values of the DRex parameters (i.e., $\lambda^* = 5$, $M^* = 125$, $\chi = 0.3$) that were identified by *Kaminski et al.* [2004] to produce matches to laboratory experimental results. LPO is assumed only to develop above 200 km depth. As described above, synthetic shear wave waveforms are produced from each geodynamic model and splitting measurements are calculated using the method of *Silver and Chan* [1991].

5.1. Radial Flow Models

[23] The first type of flow we consider is that in which the motion or shape of the underside of the lithosphere has minimal influence on the flow of the plume. The end-member for this type of flow is an axisymmetric situation in which a vertical plume rises beneath a stationary and initially flat lithosphere (GM1, Figure 8a). In this case, the model Rayleigh number is 1×10^5 and the plume has an imposed radius of 100 km and peak excess temperature of 200°C. The plume expands purely radially away from the stem due to its own buoyancy.

[24] Figures 8b–8d show the predicted pattern of flow (arrows) and seismic anisotropy (hemispheres of directional dependence of V_p) at three depths in the model. At a depth of 100 km (Figure 8b), the plume is experiencing strong radial shear near the base of the rigid lithosphere. Consequently, the olivine α-axes (direction of fastest V_p) are preferentially oriented radially away from the center of the plume and parallel to the flow. At a depth of 160 km (Figure 8d), however, the behavior is quite different. Here the flow pattern is still radial but the vertical shear because the lithosphere is small; the dominant deformation is one of contraction in the radial (the flow slows with radial distance) and vertical directions (the plume is thinning with radial distance), and circumferential elongation (flow lines are diverging). This circumferential stretching causes the olivine α-axes to preferentially align circumferentially and orthogonal to the flow [*Ito et al.*, 2011]. This result was also seen in recent laboratory experiments of plumes [*Druken et al.*, 2011]. The cross-section at depth of 140 km shows the transition in which some α-axes are primarily radial and some are primarily circumferential (Figure 8c).

[25] This layered anisotropy structure is seen by the predicted SWS (Figure 8e). The SWS that accumulates from the base of the anisotropic layer at 200 km depth, up to a depth of 140 km reflects the circumferential fast directions of the deeper portion of the plume (black tick marks, Figure 8e). The SWS pattern that accumulates from 200 km all the way to the surface shows a radial pattern of fast directions (red tick marks, Figures 8e and 8f). The layer of radial LPO is both shallower and thicker than the deeper layer with circumferentially oriented LPO, and this causes the radial pattern to dominate the SWS at the surface. Once again such a pattern is clearly inconsistent with the observed SWS pattern on Iceland (Figure 8f).

[26] The second model (GM2) is the same as model GM1 except that it simulates plate motion with a half spreading rate of 10 km/Myr. This model represents a more realistic case of plume-ridge interaction at Iceland, and one in which the flow of the plume can still be described as primarily "radial" in the sense that variations in lithosphere thickness within a few hundred km of the ridge are too small compared to the thickness of the plume to channel much flow along the ridge [*Albers and Christensen*, 2001]. The resulting flow is essentially a combination of the radial flow due to gravitational spreading of the plume plus the plate-motion induced, corner flow (Figure 9a).

[27] The predicted patterns of anisotropy and flow are shown in Figures 9b–9d. Much like the purely axisymmetric case (GM1), this case shows a dominantly circumferential pattern of fast V_p directions in the central part of the plume layer (depth of ~160 km), where vertical shear is not important (Figure 9d). With decreasing depth, the shear due to the lithosphere starts to rotate the olivine α-axes toward the spreading direction (Figures 9b and 9c). But it is worth noting that in most locations the α-axes are becoming locked in the lithosphere at a high angle to the spreading direction (e.g., at a depth of 60 km, and Y >200 km) (Figure 9b). Overall, the pattern of α-axes orientations is circumferential over a greater thickness in model GM2 than in model GM1. The two main causes are the thinner lithosphere in model GM2, and the fact that plate motion reduces the shear against the plume in the X direction.

[28] The predicted shear wave splitting directions at the surface at $Y > 50$ km show a pattern that is

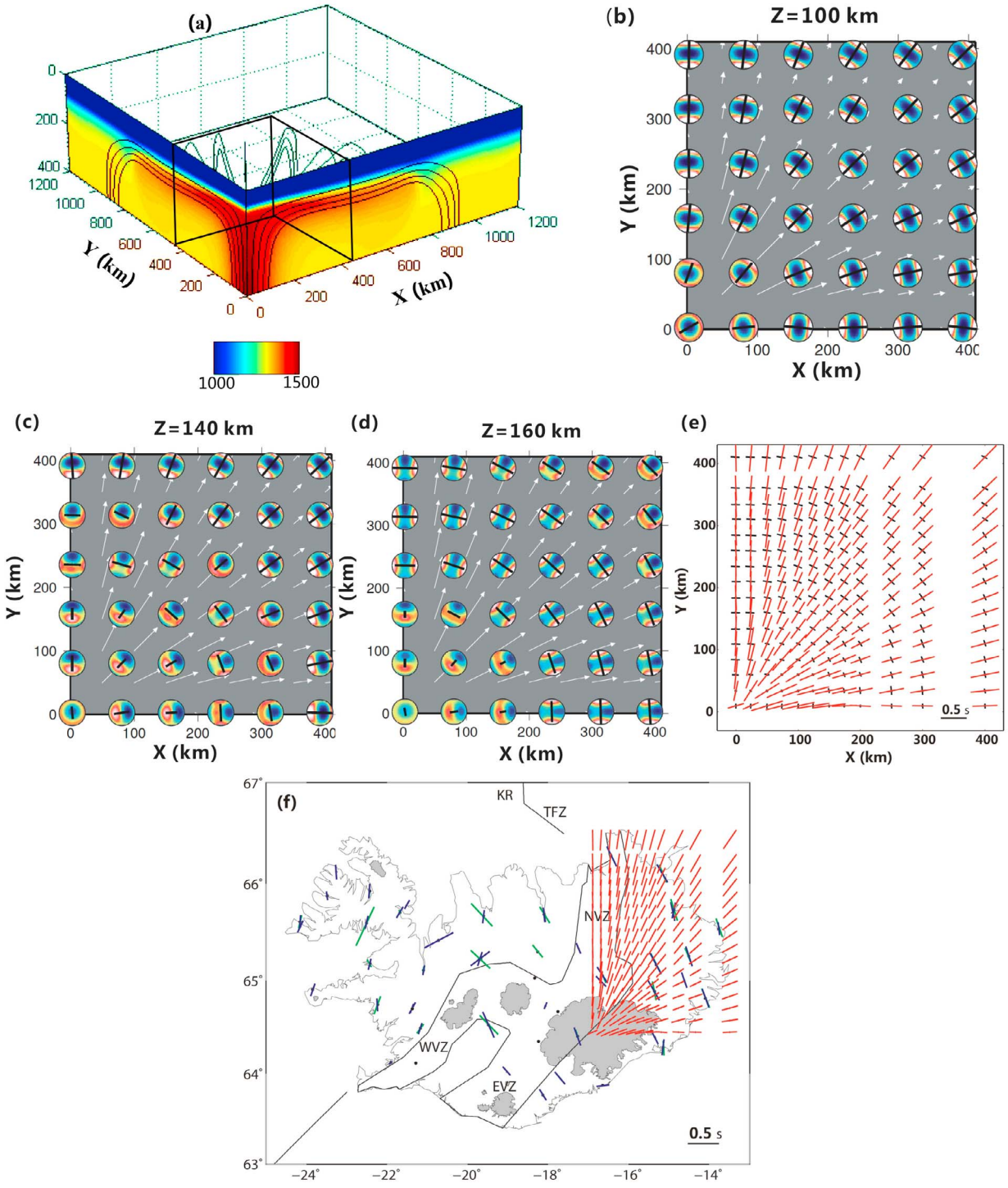

Figure 8. Perspective view of geodynamic models that simulate purely axis symmetric flow away from the plume beneath a stationary plate (GM1). (a) Model geometry. Potential temperature in °C is colored and mantle flow trajectories are shown with black lines. (b–d) Predictions of seismic anisotropy at three depths. Arrows show horizontal components of flow with length proportional to flow speed. Circles are outer hemisphere plots of the directional dependence of V_p (colors: white is fast, blue is slow). Bold bar shows the direction of the fastest V_p, which corresponds to the preferential alignment of the olivine α-axes. (e) SWS parameters obtained from the wave propagating from a depth 200 km to a depth of 140 km (black) and to the surface (red). (f) Comparison between the predicted shear wave splitting parameters at the surface (red bars) and real observations from *Bjarnason et al.* [2002] and *Li and Detrick* [2003] (blue bars) and *Xue and Allen* [2005] (green bars) in eastern Iceland.

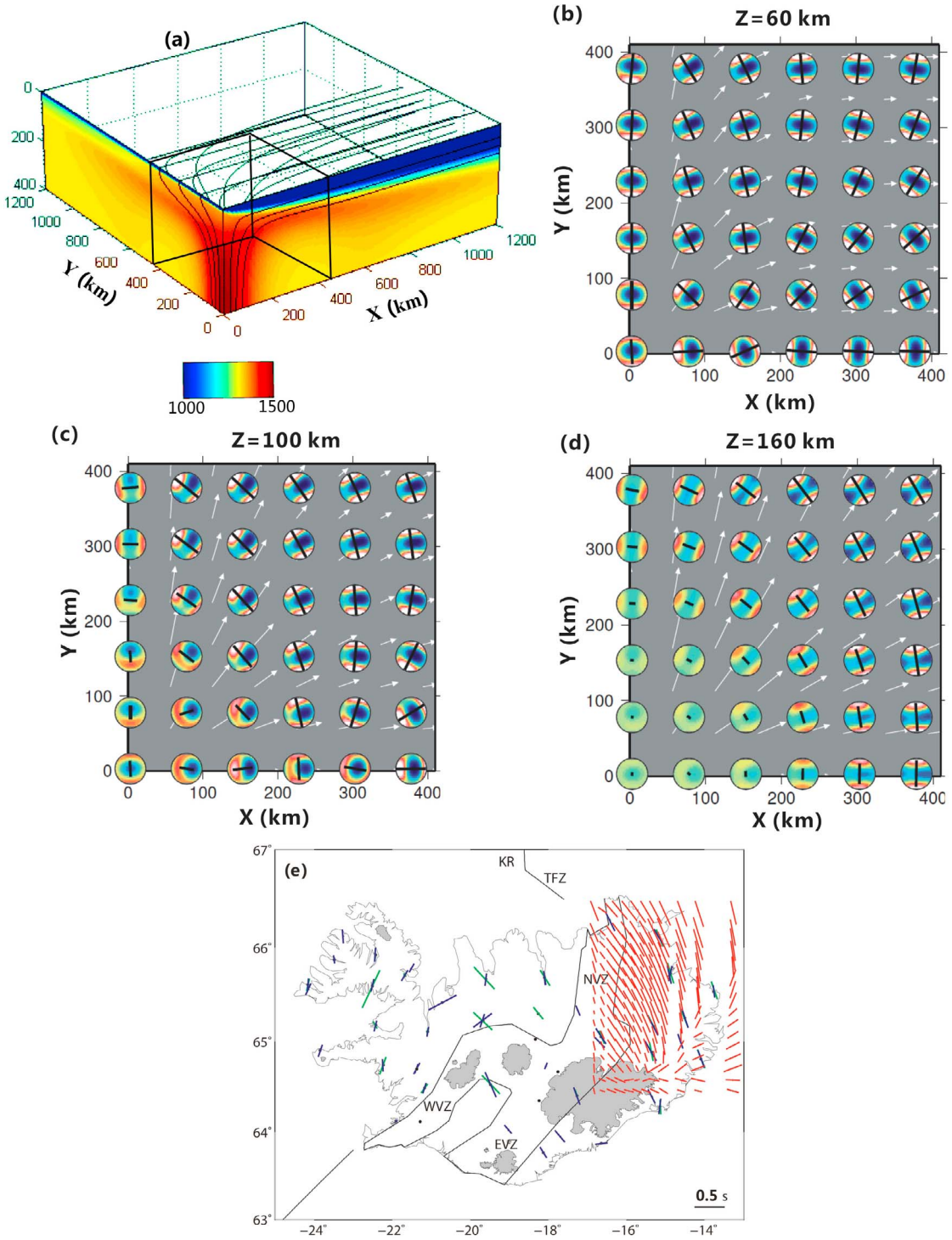

Figure 9. (a–d) The same as Figure 8 but for more realistic plume flow beneath a plate spreading at a half rate of 10 km/Myr (GM2). (e) SWS predicted at the surface (red) compared to those observed (as in Figure 8).

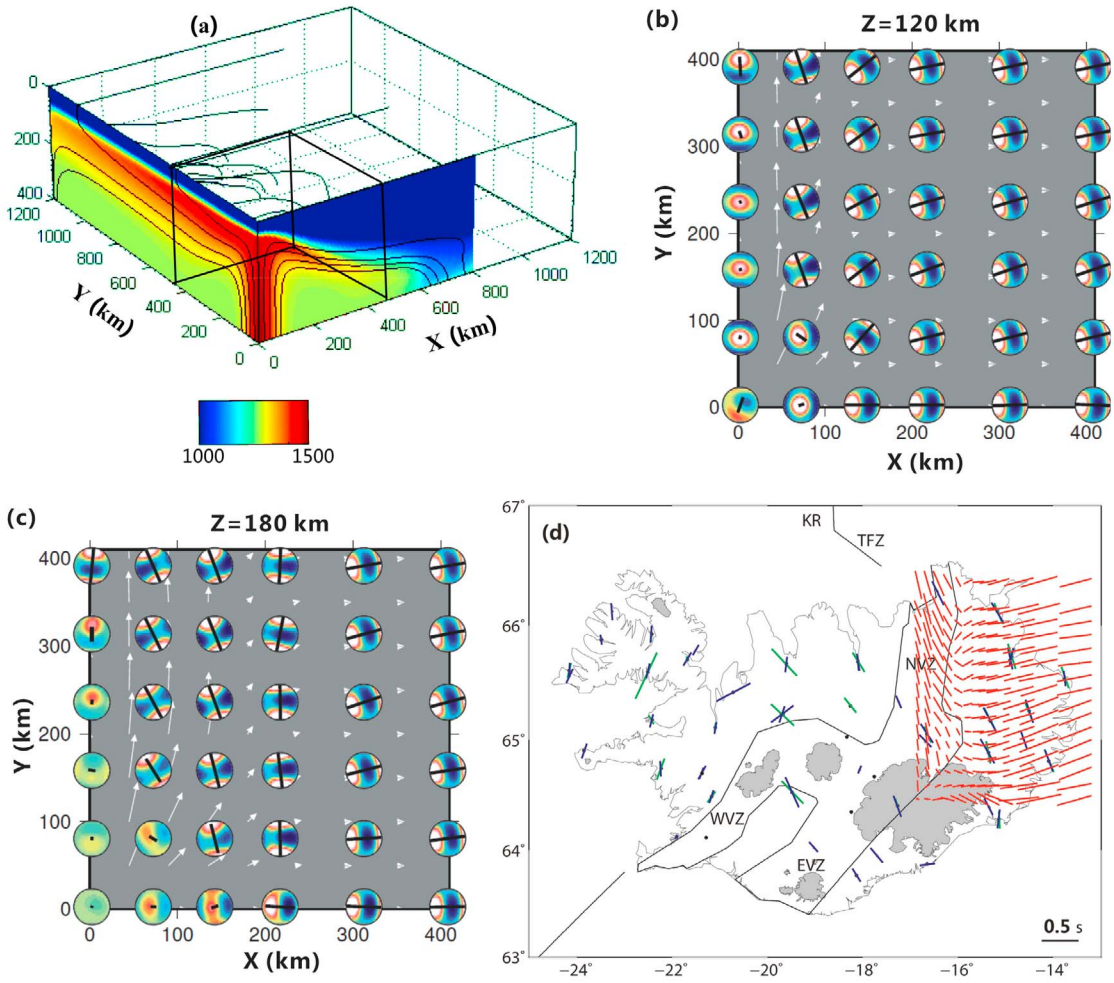

Figure 10. Same as Figure 9 but for channel flow model with unrealistic spreading rate of 1 km/Myr (GM3) and predicted anisotropy shown at two depths.

crudely circumferential about the plume (Figure 9e). It is remarkable to note that most regions in this model, especially the area within 200 km of the ridge, have fast directions of NW toward the ridge. This prediction largely agrees with the observed azimuthal anisotropy in eastern Iceland.

5.2. Channel Flow Models

[29] The next pair of models simulates a situation in which the thickening of the lithosphere away from the ridge axis channels plume material largely along the ridge axis. These models require the thickness variations of the lithosphere to be comparable to or larger than the thickness of the plume within a few hundred km of the ridge [*Albers and Christensen*, 2001].

[30] The first channel flow model (GM3) simulates an extreme case in which the plume layer is 100 km in thickness and the lithosphere thickens by even a greater amount (Figure 10a). Here the Rayleigh number of 6×10^5, peak plume temperature excess of 300°C, and plume radius of 58 km, together create a plume with large buoyancy flux but a low viscosity. A (unrealistic) plate spreading rate of only 1 km/Myr causes the lithosphere to thicken so much that it forces the plume to flow largely along the ridge. At a depth of 180 km the along-axis channeling of plume is contained within a distance of $X \sim 220$ km from the ridge axis (Figure 10c). At this depth, and directly beneath the ridge, the along-axis flow involves a weak vertical shear. Hence the olivine α-axes show a weak preferential alignment diagonally upward and along the ridge axis ($X = 0$ and $Y > 220$ km, $Z = 180$ km). Within the sides of the channel, right lateral shear becomes important and this causes the α-axes to preferentially align diagonally in a NNW sense. At distances beyond $X \sim 220$ km, where the lithosphere is present,

the α-axes are aligned more horizontally and parallel to plate motion. At a depth of 120 km (Figure 10b), the plume channel is more confined to the ridge axis and so is the transition in the pattern of LPO from beneath the ridge outward toward the lithosphere. At both depths the olivine α-axes are preferentially aligned parallel to plate motion direction east of the plume center ($Y = 0$) and X >200 km.

[31] The predicted fast split directions from this model are primarily EW to the east of the plume for $Y < 50$ km (Figure 10d). Between the EW pattern of split directions and the ridge itself, the splits are oriented primarily NW. The NW orientation of SWS is consistent with observations in east Iceland but the E-W fast directions are inconsistent with observations anywhere in Iceland.

[32] The other channel flow model (GM4) we tested has a more realistic half plate spreading rate of 10 km/Myr (Figure 11a). In order for the associated smaller, lithosphere thickness variation to channel a plume, the plume must also have a small thickness. Such a situation is created by a high Rayleigh number of 4×10^6, a plume of high excess temperature of 250°C but narrow radius of 50 km [e.g., *Ribe et al.*, 1995]. At a depth of 160 km the flow is primarily radial and the seismic anisotropy is controlled by circumferential stretching (Figure 11d). At a depth of 120 km, plate shear starts to influence the LPO far from the ridge axis by causing the olivine α-axes to rotate toward the spreading direction (Figure 11c). At a depth of 60 km, the α-axes are oriented parallel to the spreading direction within the lithosphere at $X > 200$ km. The plume channel is evident by ridge-parallel flow at $X < 150$ km ($Z = 60$ km). Near $X = 80$ km, where the right-lateral shear is strong, the olivine α-axes are preferentially oriented NW (Figure 11b).

[33] The resulting shear wave splitting pattern is shown in Figure 11e. The predicted fast splitting direction within ~75 km of the ridge for $Y < 150$ km and most of the area for $Y > 150$ km is primarily NW, toward the ridge. This pattern is roughly similar to that in the radial flow model with the same plate-spreading rate (GM2, Figure 9e) and is consistent with the observations in eastern Iceland.

6. Discussion

[34] The calculations for the simple models with imposed anisotropy suggests that anisotropy beneath western Iceland can be caused by frozen fabrics that are parallel to the abandoned ridge segments, possibly resulting from a combination of ridge-parallel melt channels and LPO due to ridge parallel flows. A thick asthenospheric layer with anisotropy that parallels the APM of the North American plate (Figures 6e and 6f) is unlikely to be present because it causes splitting directions to be roughly perpendicular to the observed anisotropy in western Iceland. For eastern Iceland, anisotropy that is directed perpendicular to the ridge axis in the lithosphere and parallel to Eurasian APM in the asthenosphere are roughly orthogonal; therefore the combined effects give a net splitting direction that cannot explain the observations in eastern Iceland (Figures 6e and 6f). The general NNW fast direction in eastern Iceland is best predicted when a layer of more northerly directed anisotropy is included in the asthenosphere (Figure 6d). A substantial layer in the asthenosphere with radially oriented LPO due to radial plume spreading produces fast SWS directions that disagree with observations, and therefore is unlikely to be present beneath Iceland.

[35] The results of the geodynamic models demonstrate that an idealized situation of purely radial flow of a plume (i.e., no plate motion) as well as an idealized situation of strong, along-axis channel flow (very slow plate motion) predict split directions that are inconsistent with the observations. Both the radial and channel flow models with a realistic spreading rate of 10 km/Myr can account for the observed shear wave splitting parameters in eastern Iceland. As these models are symmetric about the ridge axis, none of the four geodynamic models can predict the observed SWS directions in western Iceland. Future models should, for example, consider different effects such as more realistic geometry of the ridge and plume.

[36] Another important result is that the anisotropy predicted by the geodynamic models does not always parallel the direction of mantle flow, thus breaking the simplest assumption that is often used to interpret seismic anisotropy. Such a result, however, is expected given that plume-ridge interaction involves mantle deformation that is changing quickly along material flow lines, and in many places LPO does not evolve rapidly enough to keep the olivine α-axes parallel to direction of maximum elongation at infinite strain, or "infinite strain axis" [*Kaminski and Ribe*, 2002]. Although the infinite strain axis parallels the flow in steady simple shear, it does not always parallel mantle flow; in the deeper part of the ponding plume material, the outward (nearly radial) expansion causes the

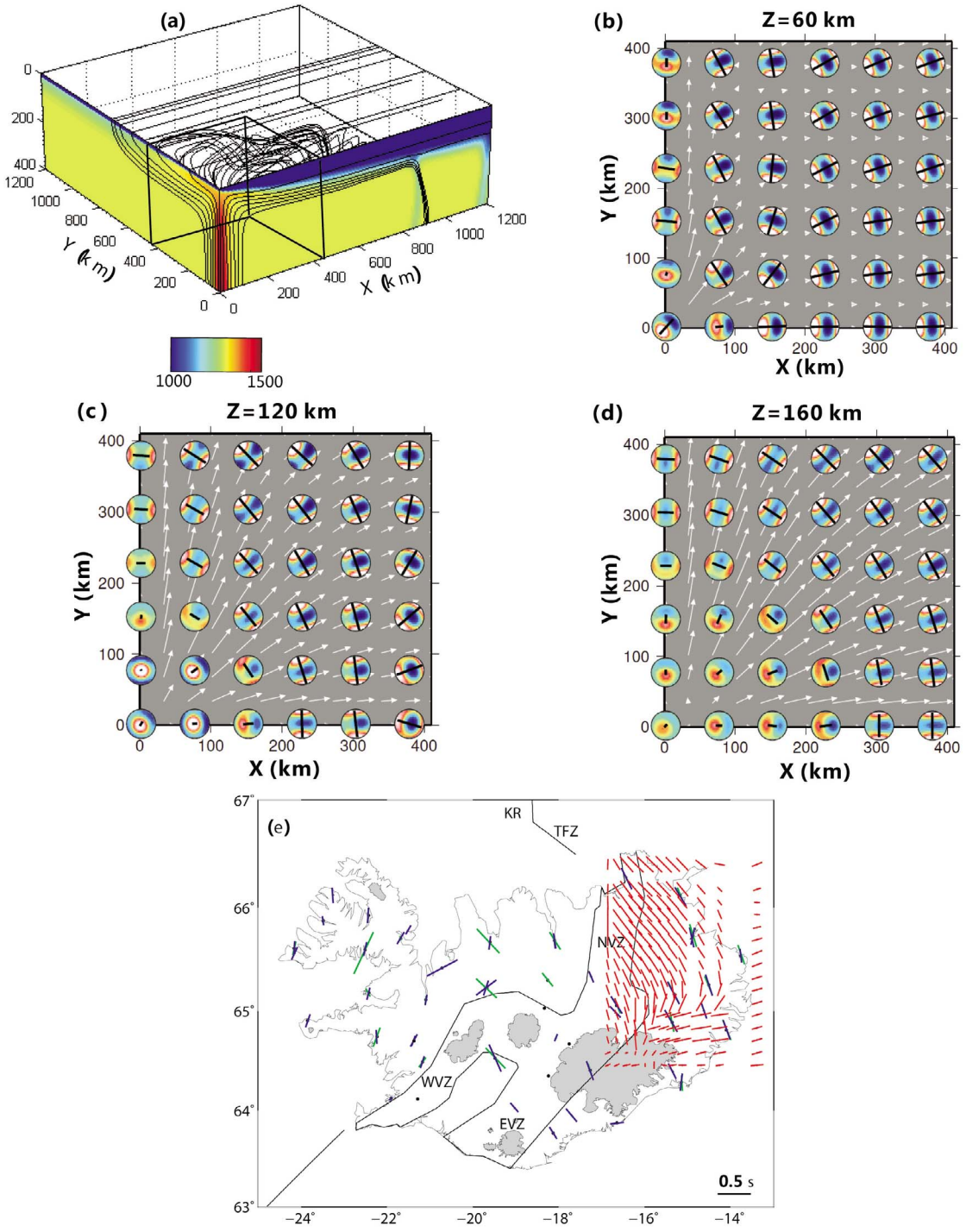

Figure 11. Same as Figure 9 but for channel flow model with realistic spreading rate of 10 km/Myr (GM4).

direction of elongation and LPO to be perpendicular to the flow.

7. Conclusions

[37] Shear wave splitting results from synthetic waveforms generated using the multidomain pseudo-spectral method agree with the analytic solution for a two-layer anisotropic model. Simple layered anisotropic models are constructed to test different idealized anisotropic structures related to factors that are related to plume ridge interaction such as plate spreading, ridge parallel fabric, absolute plate motion, ridge-channeled flow, and radial flow.

Ridge-parallel fabric in the lithosphere beneath western Iceland and a strong component of NNW LPO in the asthenosphere in eastern Iceland produce shear wave splitting results that are most consistent with the observations.

[38] Experiments with geodynamic models reveal that models with a realistic spreading rate over a range of plume viscosities and thicknesses produce a NNW direction of LPO near and to the east of the ridge. These results are consistent with observations in eastern Iceland, however, the current models predict split direction that are inconsistent with the observations in western Iceland.

Acknowledgments

[39] We thank Karen M. Fischer for good advice on shear wave splitting modeling. Most figures in this paper were made with General Mapping Tools [*Wessel and Smith*, 1998]. An anonymous reviewer and Derek Schutt provide constructive comments that help to improve this paper. This study is supported by NSF grant 0855767 to Li and Fu, and NSF grant 0855814 to Ito.

References

Abt, D. L., and K. M. Fischer (2008), Resolving three-dimensional anisotropic structure with shear wave splitting tomography, *Geophys. J. Int.*, *173*, 859–886, doi:10.1111/j.1365-246X.2008.03757.x.

Albers, M., and U. R. Christensen (2001), Channeling of plume flow beneath mid-ocean ridges, *Earth Planet. Sci. Lett.*, *187*, 207–220, doi:10.1016/S0012-821X(01)00276-X.

Ballmer, M. D., J. van Hunen, G. Ito, T. A. Bianco, and P. J. Tackley (2009), Intraplate volcanism with complex age-distance patterns: A case for small-scale sublithospheric convection, *Geochem. Geophys. Geosyst.*, *10*, Q06015, doi:10.1029/2009GC002386.

Bjarnason, I. T., C. J. Wolfe, and S. C. Solomon (1996), Initial results from the ICEMELT experiment: Body-wave delay times and shear wave splitting across Iceland, *Geophys. Res. Lett.*, *23*, 459–462, doi:10.1029/96GL00420.

Bjarnason, I. T., P. G. Silver, G. Rümpker, and S. C. Solomon (2002), Shear wave splitting across the Iceland hot spot: Results from the ICEMELT experiment, *J. Geophys. Res.*, *107*(B12), 2382, doi:10.1029/2001JB000916.

Blackman, D. K., J. M. Kendall, P. R. Dawson, H. R. Wenk, D. Boyce, and J. P. Morgan (1996), Teleseismic imaging of subaxial flow at mid-ocean ridges: Traveltime effects of anisotropic mineral texture in the mantle, *Geophys. J. Int.*, *127*, 415–426, doi:10.1111/j.1365-246X.1996.tb04730.x.

Booth, D. C., and S. Crampin (1983), The anisotropic reflectivity technique: Theory, *Geophys. J. R. Astron. Soc.*, *72*, 755–766, doi:10.1111/j.1365-246X.1983.tb02831.x.

Cerjan, C., D. Kosloff, R. Kosloff, and M. Reshef (1985), A nonreflecting boundary condition for discrete acoustic and elastic wave equations, *Geophysics*, *50*, 705–708.

Christensen, N. I. (1984), The magnitude, symmetry and origin of upper mantle anisotropy based on fabric analyses of ultrafamic tectonites, *Geophys. J. R. Astron. Soc.*, *76*, 89–111, doi:10.1111/j.1365-246X.1984.tb05025.x.

Christensen, U. (1984), Convection with pressure- and temperature-dependent non-Newtonian rheology, *Geophys. J. R. Astron. Soc.*, *77*, 343–384, doi:10.1111/j.1365-246X.1984.tb01939.x.

Druken, K. A., C. R. Kincaid, and R. W. Griffiths (2011), Surface expressions of mantle upwellings: Expect the unexpected, Abstract DI22A-03 presented at 2011 Fall Meeting, AGU, San Francisco, Calif., 5–9 Dec.

Fischer, K. M., A. Li, D. W. Forsyth, and S. Hung (2005), Imaging three-dimensional anisotropy with broadband seismometer arrays, in *Seismic Earth: Array Analysis of Broadband Seismograms*, *Geophys. Monogr. Ser.*, vol. 157, edited by A. Levander and G. Nolet, pp. 99–116, AGU, Washington, D. C., doi:10.1029/157GM07.

Fouch, M. J., P. G. Silver, D. R. Bell, and J. N. Lee (2004), Small-scale variations in seismic anisotropy near Kimberley, South Africa, *Geophys. J. Int.*, *157*, 764–774, doi:10.1111/j.1365-246X.2004.02234.x.

Francis, T. J. G. (1969), Generation of seismic anisotropy in the upper mantle along the mid-oceanic ridges, *Nature*, *221*, 162–165, doi:10.1038/221162b0.

Fu, Y. V., et al. (2008), Indian mantle corner flow at southern Tibet revealed by shear wave splitting measurements, *Geophys. Res. Lett.*, *35*, L02308, doi:10.1029/2007GL031753.

Gripp, A. G., and R. G. Gordon (1990), Current plate velocities relative to the hotspots incorporating the NUVEL-1 global plate motion model, *Geophys. Res. Lett.*, *17*, 1109–1112.

Hardarson, B. S., J. G. Fitton, R. M. Ellam, and M. S. Pringle (1997), Rift relocation—A geochemical and geochronological investigation of a paleorift in northwest Iceland, *Earth Planet. Sci. Lett.*, *153*, 181–196, doi:10.1016/S0012-821X(97)00145-3.

Hirth, G., and D. L. Kohlstaedt (2003), Rheology of the upper mantle and the mantle wedge: A view from the experimentalists, in *Inside the Subduction Factory*, *Geophys. Monogr. Ser.*, vol. 138, edited by J. Eiler, pp. 83–105, AGU, Washington, D. C., doi:10.1029/138GM06.

Hung, S., and D. W. Forsyth (1998), Modelling anisotropic wave propagation in oceanic inhomogeneous structures using the parallel multidomain pseudo-spectral method, *Geophys. J. Int.*, *133*, 726–740, doi:10.1046/j.1365-246X.1998.00526.x.

Hung, S., and D. W. Forsyth (1999), Anisotropy in the oceanic lithosphere from the study of local intraplate earthquakes on the west flank of the southern East Pacific Rise: Shear wave splitting and waveform modeling, *J. Geophys. Res.*, *104*, 10,695–10,717.

Hung, S., D. W. Forsyth, and D. R. Toomey (2000), Can a narrow, melt-rich, low-velocity zone of mantle upwelling be hidden beneath the East Pacific Rise? Limits from waveform modeling and the MELT Experiment, *J. Geophys. Res.*, *105*, 7945–7960.

Ito, G. (2001), Reykjanes 'V'-shaped ridges originating from a pulsing and dehydrating mantle plume, *Nature*, *411*, 681–684, doi:10.1038/35079561.

Ito, G., J. Lin, and C. W. Gable (1996), Dynamics of mantle flow and melting at a ridge-centered hotspot: Iceland and the Mid Atlantic ridge, *Earth Planet. Sci. Lett.*, *144*, 53–74, doi:10.1016/0012-821X(96)00151-3.

Ito, G., R. Dunn, Y. V. Fu, A. Gallego, A. Li, and C. J. Wolfe (2011), Mantle flow and seismic anisotropy associated with plume-plate interaction, Abstract DI51C-07 presented at 2011 Fall Meeting, AGU, San Francisco, Calif., 5–9 Dec.

Kaminski, È., and N. M. Ribe (2002), Timescales for the evolution of seismic anisotropy in mantle flow, *Geochem. Geophys. Geosyst.*, *3*(8), 1051, doi:10.1029/2001GC000222.

Kaminski, È., N. M. Ribe, and J. T. Browaeys (2004), D-Rex, a program for calculation of seismic anisotropy due to crystal lattice preferred orientation in the convective upper mantle, *Geophys. J. Int.*, *158*, 744–752, doi:10.1111/j.1365-246X.2004.02308.x.

Kendall, J. M., and C. J. Thomson (1993), Maslov ray summation, pseudo-caustics, Lagrangian equivalence and transient seismic waveforms, *Geophys. J. Int.*, *113*, 186–214, doi:10.1111/j.1365-246X.1993.tb02539.x.

Kind, R., et al. (1985), Observations of laterally inhomogeneous anisotropy in the continental lithosphere, *Nature*, *318*, 358–361, doi:10.1038/318358a0.

Li, A., and R. S. Detrick (2003), Azimuthal anisotropy and phase velocity beneath Iceland: Implication for plume-ridge interaction, *Earth Planet. Sci. Lett.*, *214*, 153–165, doi:10.1016/S0012-821X(03)00382-0.

Li, A., and R. S. Detrick (2006), Seismic structure of Iceland from Rayleigh wave inversions and geodynamic implications, *Earth Planet. Sci. Lett.*, *241*, 901–912, doi:10.1016/j.epsl.2005.10.031.

Mainprice, D., and P. G. Silver (1993), Interpretation of SKS waves using samples from the subcontinental lithosphere, *Phys. Earth Planet. Inter.*, *78*, 257–280, doi:10.1016/0031-9201(93)90160-B.

Moresi, L., and M. Gurnis (1996), Constraints on the lateral strength of slabs from three-dimensional dynamic flow models, *Earth Planet. Sci. Lett.*, *138*, 15–28, doi:10.1016/0012-821X(95)00221-W.

Ribe, N. M., U. R. Christensen, and J. Theissing (1995), The dynamics of plume-ridge interaction, 1: Ridge-centered plumes, *Earth Planet. Sci. Lett.*, *134*, 155–168.

Rümpker, G., and P. G. Silver (1998), Apparent shear wave splitting parameters in the presence of vertically varying anisotropy, *Geophys. J. Int.*, *135*, 790–800.

Sæmundsson, K. (1974), Evolution of the axial rifting zone in northern Iceland and the Tjörnes fracture zone, *Geol. Soc. Am. Bull.*, *85*, 495–504.

Silver, P. G. (1996), Seismic anisotropy beneath the continents: Probing the depths of geology, *Annu. Rev. Earth Planet. Sci.*, *24*, 385–432, doi:10.1146/annurev.earth.24.1.385.

Silver, P. G., and W. W. Chan (1988), Implications for continental structure and evolution from seismic anisotropy, *Nature*, *335*, 34–39, doi:10.1038/335034a0.

Silver, P. G., and W. W. Chan (1991), Shear wave splitting and subcontinental mantle deformation, *J. Geophys. Res.*, *96*, 16,429–16,454, doi:10.1029/91JB00899.

Silver, P. G., and M. K. Savage (1994), The interpretations of shear wave splitting parameters in the presence of two anisotropic layers, *Geophys. J. Int.*, *119*, 949–963, doi:10.1111/j.1365-246X.1994.tb04027.x.

Vinnik, L. P., V. Farra, and B. Romanowicz (1989), Azimuthal anisotropy in the Earth from observations of SKS at GEOSCOPE and NARS broadband stations, *Bull. Seismol. Soc. Am.*, *79*, 1542–1558.

Vinnik, L. P., L. I. Makeyeva, A. Milev, and A. Y. Usenko (1992), Global patterns of azimuthal anisotropy and deformations in the continental mantle, *Geophys. J. Int.*, *111*, 433–447, doi:10.1111/j.1365-246X.1992.tb02102.x.

Vogt, P. R. (1976), Plumes, subaxial pipe flow, and topography along the mid-oceanic ridge, *Earth Planet. Sci. Lett.*, *29*, 309–325, doi:10.1016/0012-821X(76)90135-7.

Wessel, P., and W. H. F. Smith (1998), New, improved version of the Generic Mapping Tools released, *Eos Trans. AGU*, *79*, 579, doi:10.1029/98EO00426.

White, N., and B. Lovell (1997), Measuring the pulse of a plume with the sedimentary record, *Nature*, *387*, 888–891, doi:10.1038/43151.

Wolfe, C. J., and P. G. Silver (1998), Seismic anisotropy of oceanic upper mantle: Shear wave splitting methodologies and observations, *J. Geophys. Res.*, *103*, 749–771, doi:10.1029/97JB02023.

Xue, M., and R. M. Allen (2005), Asthenospheric channeling of the Icelandic upwelling: Evidence from seismic anisotropy, *Earth Planet. Sci. Lett.*, *235*, 167–182, doi:10.1016/j.epsl.2005.03.017.

Yale, M. M., and J. P. Morgan (1998), Asthenosphere flow model of hotspot-ridge interactions: A comparison of Iceland and Kerguelen, *Earth Planet. Sci. Lett.*, *161*, 45–56, doi:10.1016/S0012-821X(98)00136-8.

Yardley, G. S., and S. Crampin (1991), Extensive-dilatancy anisotropy: Relative information in VSPs and reflection surveys, *Geophys. Prospect.*, *39*, 337–355, doi:10.1111/j.1365-2478.1991.tb00316.x.

Zhang, S., and S. Karato (1995), Lattice preferred orientation of olivine aggregates deformed in simple shear, *Nature*, *375*, 774–777, doi:10.1038/375774a0.

Zhong, S., M. T. Zuber, L. Moresi, and M. Gurnis (2000), Role of temperature-dependent viscosity and surface plates in spherical shell models of mantle convection, *J. Geophys. Res.*, *105*, 11,063–11,082, doi:10.1029/2000JB900003.